8th International IEEE EMBS Conference on Neural Engineering
Shanghai, China, May 25 - 28 , 2017

Modeling Motor Responses of Paraplegics under Epidural Spinal Cord Stimulation*

Ellen R. Feldman and Joel W. Burdick[1]

Abstract— **Epidural spinal cord stimulation (SCS) is a promising therapy for spinal cord injury (SCI). This paper combines experimental data from epidurally-stimulated human paraplegic patients with computational models of SCS to identify the electric field features correlated with the patients' ability to stand. We locate the spinal cord regions most critical to stimulated standing and find that the most informative stimulating features agree with results from nerve fiber theory. Further applications of our work include developing algorithms to optimize stimulation configurations for SCI patients, determining optimal electrode placement, and considering novel electrode array designs.**

I. INTRODUCTION

Spinal cord injury (SCI) is a debilitating condition associated with damage to motor, sensory, and autonomic systems. Recently, spinal cord stimulation (SCS) via multi-electrode arrays placed in the epidural space over the lumbosacral cord has emerged as a promising therapy. This approach enables human paraplegic patients to stand and regain partial control of leg movements [1], while making gains in lost autonomic function. The success of this method is due in part to the excitation of postural control and central pattern generator circuitry in the spinal cord [2], although the exact mechanisms behind it remain uncertain.

This study involves data collected from two paraplegic patients implanted with 16-electrode epidural arrays, shown in Fig. 1. These stimulators have several modifiable parameters: the choice of active electrodes, their polarities (positive, negative, or neutral), and the amplitude, frequency, and pulse width of the pulse trains applied to the active electrodes (see Fig. 2). The choice of electrode polarities alone yields a search space of $3^{16} \approx 4.3 \times 10^7$ possible configurations. Not only must these parameters be optimized for each patient, but their optimal values may vary over time. Machine learning methods can efficiently search this intractably-large space to locate optimal stimulation configurations [3], [4], [5].

Various studies [6], [7], [8] utilize computational models to simulate electrical activity due to SCS and its impact upon the nervous system. A few studies (e.g. Barolat [6] and Capogrosso et al. [7]) relate such simulations to empirical data. Barolat validates a computational model by comparing it with pain response data from subjects implanted with epidural electrodes. Capogrosso et al. apply computational models to predict optimal positions for epidural electrodes.

*This work was supported by the National Science Foundation, the National Institutes of Health, and the Christopher and Dana Reeve Foundation.

[1]E. Feldman and J. Burdick are with the Division of Engineering and Applied Science at the California Institute of Technology, Pasadena, CA 91125, USA {efeldman, jburdick}@caltech.edu

This paper links computational models of epidural SCS to experimental data obtained by testing paraplegic patients' standing performance under different stimulation parameters. Each stimulus is simulated to estimate the electrical activity in the spinal cord and surrounding tissues near the implant under that stimulation. Examined via regression and feature selection techniques, the simulation results help to explain the empirical performance of the stimuli in the patients, identifying the electric field features which best enable prediction of patient motor responses, as well as spinal cord regions which may be most important to stimulate.

The methods introduced in this paper should allow for improved design of epidural stimulating electrodes specialized for SCS in cases of paralysis and shed more light upon mechanisms underlying recovery of function in SCI via SCS.

II. DATA COLLECTION

The empirical dataset was collected from two chronic paraplegics (given codes ATC and ARI) implanted with Medtronic Specify™ 5-6-5 electrode arrays, as shown in Fig. 1. As measured by electromyography, neither patient could achieve volitional leg muscle control without stimulation.

Experiments were performed over two non-consecutive weeks for each patient, with 117 stimulation patterns tested in ATC (July 2014 and January 2015) and 90 patterns tested in ARI (March 2014 and August 2014); the number of stimuli was determined by experimental time and patient fatigue. During each ∼5-minute trial, the patient attempted to stand in a frame, as pictured in Fig. 3, under the fixed stimulus. The stimulation amplitude was adjusted for each patient, while the frequency (25 Hz) and pulse width (200 μsec) were held constant. The stand frame and trainers provided support and assistance as needed.

Electrode configurations were selected using a Rank-Comparison algorithm [4], which searches for optimal parameters while balancing exploration and exploitation. Both patients achieved full weight-bearing standing with minimal assistance under their empirically-optimal stimulation. A clinician scored the patients' responses to the stimuli on a 1-10 scale; with increasing score, the patient gains independence and stability, while improving in performance and duration, with a score of 6 marking the threshold for independent standing. The algorithm optimizes this score.

III. SIMULATIONS

This study compares the performance of SCS in human patients with simulations of the same stimuli, performed using COMSOL Multiphysics®. We aim to identify those

978-1-5090-4603-4/17/$31.00 ©2017 IEEE

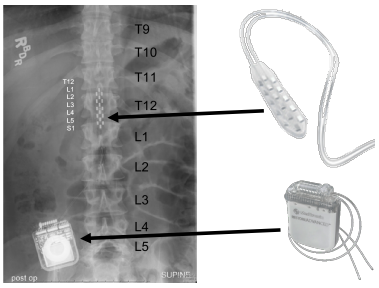

Fig. 1. CT Scan from a patient implanted with a Medtronic Specify™ 5-6-5 electrode array; the array and impulse generator are enlarged.

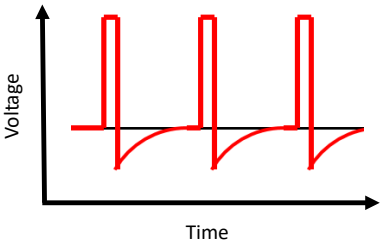

Fig. 2. Sketch of a positive-polarity stimulation waveform from the electrode array.

Fig. 3. Patient standing with epidural spinal cord stimulation.

stimulating electric field properties leading to the best standing performance, and to learn whether the simulations can help to illuminate neural mechanisms underlying SCS. This section discusses the simulation methodology; the technical report [9] also contains further details.

Our study follows the method of Ladenbauer (2008) [8], which models the electrodes and anatomical structures as a *volume conductor*. Our model (see Fig. 4a-4b) includes gray matter, white matter, cerebrospinal fluid (CSF), dura mater, epidural fat, vertebral bone, intervertebral discs, ligaments, a thoracic/abdominal compartment, skin, and subcutaneous fat. The tissues' electrical conductivities were calculated at 40Hz using data from Gabriel (1996) [10]. The electrical activity due to stimulation is concentrated near the array placed within the epidural fat; thus, we approximate the outer body boundary as a rectangular prism. The volume conductor is then partitioned into a mesh as in Fig. 4c, over which the finite element method numerically solves Laplace's equation:

$$\nabla \cdot (\sigma \nabla V) = 0, \tag{1}$$

where V is electric potential and σ is electrical conductivity. Laplace's equation provides a quasi-static approximation of Poisson's equation; this assumes negligible capacitive effects in bodily tissue, as demonstrated experimentally by Schwan and Kay [11] at frequencies below 1 kHz.

We use Dirichlet boundary conditions to set the voltages at active electrode surfaces and a Neumann boundary condition to prevent current from leaving the volume conductor:

$$V(x) = V_0(\vec{x}),\ \vec{x} \in \Gamma_D, \tag{2}$$

$$\vec{J}(\vec{x}) \cdot \vec{n} = (-\sigma \nabla V(\vec{x})) \cdot \vec{n} = \vec{0},\ \vec{x} \in \Gamma_N, \tag{3}$$

where Γ_D is the set of points comprising the electrode surfaces, Γ_N is the volume conductor's outer boundary, $\vec{J}$ is current density, and $\vec{n}$ is a unit vector normal to Γ_N.

Each stimulation pattern in the experimental dataset was simulated, yielding a voltage distribution throughout the volume conductor. As justified by Schwan and Kay [11] and Ladenbauer [8], we only simulate the effect of the stimulus' pulse at its peak. Fig. 4d illustrates an example simulation.

IV. RESULTS

A. Feature Extraction

Features are extracted from the simulation results by dividing a region of interest into voxels. The region is a bounding box that encompasses the main activity generated by the array, extending laterally 3mm beyond the CSF to include the dorsal roots, and vertically 5mm above and below the electrodes. To account for voxel partitioning effects, we considered voxels of five sizes; edge lengths are $\{s,\ 1.5s,\ 2s,\ 3s,\ 4s\}$, $s \approx 1.4$mm (see Fig. 5), yielding $\{264,\ 672,\ 2,112,\ 5,376,\ 16,896\}$ voxels respectively. For each voxel, we extract average values for the voltage, 3×1 voltage gradient (4), and six unique entries of the voltage Hessian matrix (5) to produce 10 unique features per voxel:

$$\nabla V = \begin{bmatrix} \frac{\partial V}{\partial x} & \frac{\partial V}{\partial y} & \frac{\partial V}{\partial z} \end{bmatrix} = -\vec{E} \tag{4}$$

$$\nabla^2 V = \begin{bmatrix} \frac{\partial^2 V}{\partial x^2} & \frac{\partial^2 V}{\partial x \partial y} & \frac{\partial^2 V}{\partial x \partial z} \\ \frac{\partial^2 V}{\partial y \partial x} & \frac{\partial^2 V}{\partial y^2} & \frac{\partial^2 V}{\partial y \partial z} \\ \frac{\partial^2 V}{\partial z \partial x} & \frac{\partial^2 V}{\partial z \partial y} & \frac{\partial^2 V}{\partial z^2} \end{bmatrix}. \tag{5}$$

The Hessian values are of interest, as a neuron's activating function $f(x)$ (6) [12] predicts that its behavior is proportional to the second spatial derivative of the extracellular voltage V_e along the axon. If $f(x)$ is sufficiently large, an action potential is expected to originate at its maximum [8].

$$f(x) \propto \frac{\partial^2 V_e}{\partial x^2} \tag{6}$$

B. Regression Model Evaluation

For each of the four datasets (2 patients, 2 weeks of testing each), we examined the features' ability to predict patient responses using random forest (RF) [13] and elastic net (EN) regression [14], with the features as predictor variables and response scores as targets. The RFs have $8,000$ trees, where each tree has a minimum leaf node size of 3 and considers one-third of the features at each split; the EN regularization coefficients, meanwhile, were optimized via 10-fold cross-validation for each dataset and voxel size individually. Model predictions were cross-validated via out-of-bag predictions for RFs and leave-one-out cross validation for ENs (e.g. Fig. 6). We calculated the p-values associated with the Pearson's correlation coefficients between response scores and model predictions (shown in Fig. 7). Correlations are significant at the 0.05 level in three of four cases, though not in ARI's August experiment. ARI was unable to train for the three preceding months due to medical complications, which may have influenced this result, as variability in motor skill learning decreases with training in healthy humans [15].

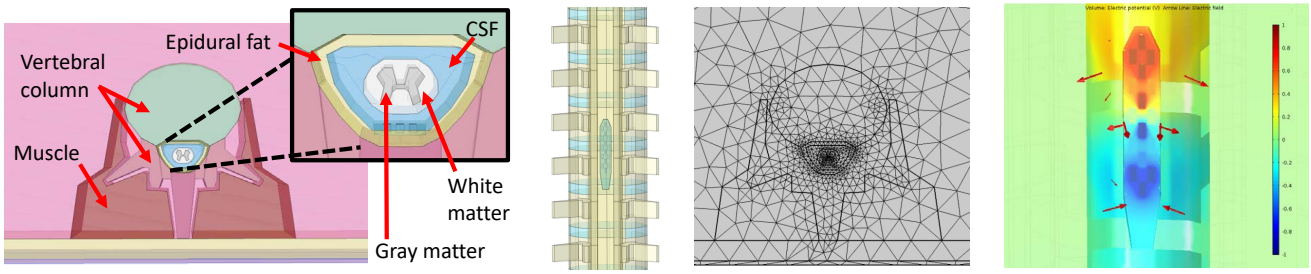

(a) (b) (c) (d)

Fig. 4. Volume conductor model. a) Top view. b) Vertebral column, with electrode array inside the epidural fat. c) Finite element method mesh. d) Voltage distribution and electric field lines (red arrows) for an example simulation; red denotes positive voltage, blue is negative.

C. Feature Selection

To better understand the relationship between the features and patient responses, we analyze which features are most important in score prediction via the following approaches:

1) RF regression: permute a feature's values across out-of-bag samples in each tree, and average the trees' changes in prediction error [13]. More important features yield greater error increases when thus permuted.
2) EN regression: regularization induces a sparse coefficient vector. More important features require greater regularization to force their coefficients to zero.
3) Mutual information (MI): more informative predictor variables have a higher MI with the target variable. We approximate MI via kernel density estimation.

To compare these methods, we compute the Pearson's correlation coefficient p-values between their resulting vectors of feature importance values. This procedure involves 60 comparisons total (3 pairwise comparisons among the 3 methods for each of the 4 datasets and 5 voxel sizes). All but two of the resulting 60 p-values are significant at the 0.05 level, of which 50 are below 10^{-20}. The strong correlations between these three different methods highlights commonalities in their interpretations of the data.

We identify the most significant feature importance estimates by determining a threshold upon the RF importance measurements. For uninformative features, this method yields values symmetrically distributed about 0; the most important features form an upper tail exceeding the symmetric portion of the distribution. We extract this tail as shown in Fig. 8, via a distance-based outlier detection technique [16]: a value is labeled as an outlier if at least fraction p of values lie a distance D or greater from it (with tuned parameters $D = 0.007$ and $p = (n - 15)/n$, where n is the number of features). By this procedure, the most important features are selected for each dataset and voxel size.

V. DISCUSSION

This work demonstrates that features extracted from SCS simulations can inform us about paraplegic patients' resultant ability to stand; in three of four cases, the regression models effectively predict clinicians' scores. Furthermore, three feature importance measures correlate strongly with one another, which emphasizes their significance. To gain insight into the nervous system's response to SCS, this section investigates the types and locations of features that most influence patient responses.

A. Locating Spinal Cord Areas Most Critical for Stimulation

A patient's response to SCS likely depends most upon electrical activity in anatomical regions containing the most important features. To verify that these locations are invariant with respect to voxel boundaries, we test whether important features occur in similar regions as voxel size changes.

We define each voxel's importance as the maximum importance among its 10 features, and important voxels as those with above-threshold importance. For each voxel size, important voxels are compared against results for each other size, giving 20 comparisons per week of testing. To compare voxels of sizes A and B, we find the importance values of all size-B voxels that physically overlap with size-A important voxels; then, we calculate the probability that if a group of the same number of size-B voxels were drawn uniformly at random from all size-B voxels, their importance values would rank at least as highly. These probabilities, equivalent to Wilcoxon rank-sum test p-values, are displayed in Fig. 9, and most are significant at the 0.05 level.

While similar regions remain important as voxel size varies, the most important regions may differ across datasets. In patient ATC's July data, the important features are concentrated slightly below the array's vertical midpoint, as depicted in Fig. 10; however, in ATC's January data, the important features are clustered near the upper electrodes.

B. Hessian (2nd-Derivative) Features are Most Important

When visualizing important features as in Fig. 10, Hessian features consistently appear the most. We test the hypothesis that Hessian features are indeed more important than voltages or their gradients by calculating, for each group of selected important features, the probability that at least the observed number of Hessian values would appear in a randomly-drawn group of features of the same size. All 20 of these probabilities (one per week of testing and voxel size) are of order 10^{-3} or lower, and thus significant at the 0.05 level.

This result implies that the voltage Hessian most directly affects the patient's response, which corresponds with nerve fiber theory as the second voltage derivative appears in the neural activating function (6). Furthermore, Hessian features add significant information to the stimulation parameters, which are captured by voltage values near the array's surface.

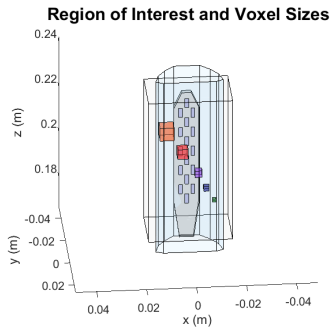

Fig. 5. Sketch of the implant and CSF, with the region of interest (large rectangular prism) and 5 voxel sizes used for feature extraction.

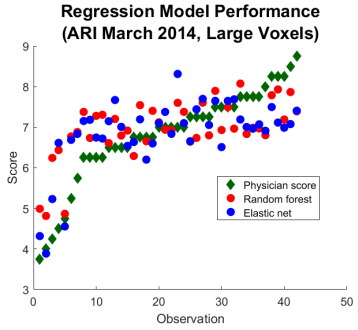

Fig. 6. Cross-validated regression predictions: out-of-bag prediction for the random forest and leave-one-out prediction for the elastic net.

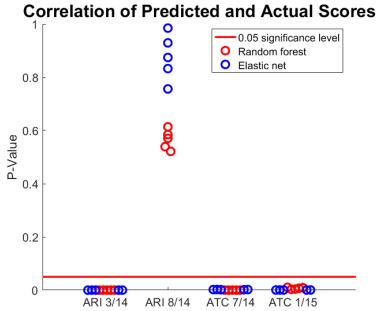

Fig. 7. Correlation p-values between cross-validated predictions and clinicians' scores. Separate points are drawn for each voxel size.

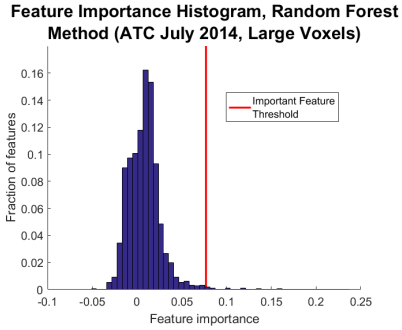

Fig. 8. Histogram of feature importance values with the outlier threshold marked, for ATC July 2014 and the largest voxel size.

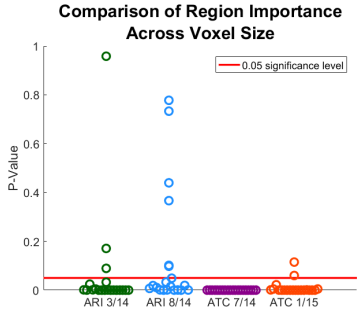

Fig. 9. Test of region importance similarity across voxel size; each voxel size pair is considered twice, as the test is asymmetric.

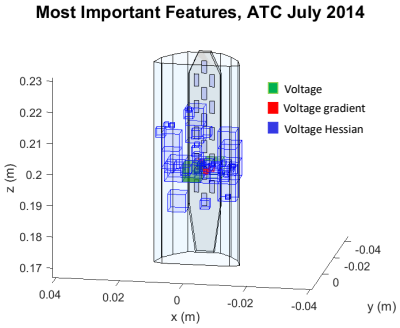

Fig. 10. Most important features for ATC July 2014 data and voxel edge lengths $\{s, 2s, 4s\}$, $s \approx 1.4$mm, as described in Section IV-A.

C. Conclusion

This work connects an empirical study with two paraplegic patients to computational simulations examining the effect of epidural SCS upon surrounding tissue. Analyzing the simulated electrical activity, we identify features that help to predict stimulation performance, which may point toward spinal cord regions most critical to stimulation success. Voltage Hessian features are found to be more informative than either the voltages or electric field, as suggested by the neural activating function. We are applying this work toward searching for optimal stimuli, which could improve online algorithms for suggesting stimuli in response to sequentially-acquired patient data. Such modeling could also help to locate neural mechanisms which contribute to the SCI patient's recovery, providing new insight into the nervous system's response to SCS. Furthermore, it could aid in electrode placement and array design, facilitating optimization of such parameters as the number of electrodes and their shapes.

ACKNOWLEDGMENT

We are grateful to Yanan Sui for collecting and sharing the experimental dataset and for many helpful conversations.

REFERENCES

[1] S. Harkema, Y. Gerasimenko, J. Hodes, J. Burdick *et al.*, "Effect of epidural stimulation of the lumbosacral spinal cord on voluntary movement, standing, and assisted stepping after motor complete paraplegia: A case study," *The Lancet*, vol. 377, no. 9781, pp. 1938–1947, 2011.

[2] M. R. Dimitrijevic, Y. Gerasimenko, and M. M. Pinter, "Evidence for a spinal central pattern generator in humans," *Annals of the New York Academy of Sciences*, vol. 860, no. 1, pp. 360–376, 1998.

[3] T. Desautels, A. Krause, and J. W. Burdick, "Parallelizing exploration-exploitation tradeoffs in Gaussian process bandit optimization," *J. Machine Learning Research*, vol. 15, no. 1, pp. 3873–3923, 2014.

[4] Y. Sui and J. Burdick, "Clinical online recommendation with subgroup rank feedback," in *Proc. ACM Conf. on Rec. Sys.*, 2014, pp. 289–292.

[5] Y. Sui, A. Gotovos, J. Burdick, and A. Krause, "Safe exploration for optimization with Gaussian processes," in *Proc. 32nd Int. Conf. Machine Learning*, 2015, pp. 997–1005.

[6] G. Barolat, "Epidural spinal cord stimulation: Anatomical and electrical properties of the intraspinal structures relevant to spinal cord stimulation and clinical correlations," *Neuromodulation: Technology at the Neural Interface*, vol. 1, no. 2, pp. 63–71, 1998.

[7] M. Capogrosso, N. Wenger, S. Raspopovic *et al.*, "A computational model for epidural electrical stimulation of spinal sensorimotor circuits," *J. Neuroscience*, vol. 33, no. 49, pp. 19 326–19 340, 2013.

[8] J. Ladenbauer, "Simulation of the excitation of human lower spinal cord structures with surface electrodes: 3D finite element analysis and nerve fiber modeling," Master's thesis, Vienna Univ. Techn., 2008.

[9] E. Feldman and J. Burdick, "Modeling motor responses of paraplegics under epidural spinal cord stimulation: Computational modeling technical report," California Institute of Technology, Tech. Rep., 2017.

[10] C. Andreuccetti *et al.*, "An Internet resource for the calculation of the dielectric properties of body tissues in the frequency range 10 Hz - 100 GHz," http://niremf.ifac.cnr.it/tissprop/, iFAC-CNR, Florence (Italy), 1997. Based on data published by C. Gabriel et al. in 1996.

[11] H. P. Schwan and C. F. Kay, "Capacitive properties of body tissues," *Circulation Research*, vol. 5, no. 4, pp. 439–443, 1957.

[12] F. Rattay, "The basic mechanism for the electrical stimulation of the nervous system," *Neuroscience*, vol. 89, no. 2, pp. 335–346, 1999.

[13] T. Hastie, R. Tibshirani, and J. Friedman, *The Elements of Statistical Learning: Data Mining, Inference, and Prediction*. Springer, 2011.

[14] H. Zou and T. Hastie, "Regularization and variable selection via the elastic net," *Journal of the Royal Statistical Society: Series B (Statistical Methodology)*, vol. 67, no. 2, pp. 301–320, 2005.

[15] L. Shmuelof, J. W. Krakauer, and P. Mazzoni, "How is a motor skill learned? Change and invariance at the levels of task success and trajectory control," *J. Neurophy.*, vol. 108, no. 2, pp. 578–594, 2012.

[16] M. Breunig *et al.*, "Lof: identifying density-based local outliers," in *ACM sigmod record*, vol. 29, no. 2. ACM, 2000, pp. 93–104.